ISSN 1063-7826, Semiconductors, 2018, Vol. 52, No. 16, pp. 2073–2077. © Pleiades Publishing, Ltd., 2018.

26th INTERNATIONAL SYMPOSIUM "NANOSTRUCTURES: PHYSICS AND TECHNOLOGY". NANOSTRUCTURE CHARACTERIZATION

Growth of Textured Au–Fe/Fe Hybrid Nanocrystals on Oxidized Silicon Surface[1]

I. A. Tarasov[a,*], T. E. Smolyarova[a,b], I. A. Yakovlev[a], N. N. Kosyrev[a,c], V. A. Komarov[a,b], I. V. Nemtsev[d], S. N. Varnakov[a], S. G. Patrin[a,b], and S. G. Ovchinnikov[a,b]

[a] *Kirensky Institute of Physics, Federal Research Center KSC SB RAS, Krasnoyarsk, 660036 Russia*
[b] *Siberian Federal University, Krasnoyarsk, 660041 Russia*
[c] *Achinsk Branch of Krasnoyarsk State Agrarian University, Achinsk, 662150 Russia*
[d] *Federal Research Center KSC Siberian Branch Russian Academy of Sciences, Krasnoyarsk, 660036 Russia*
**e-mail: tia@iph.krasn.ru*

Abstract—We present in this report the route to produce highly-textured $Au_3Fe(111)/Fe(110)$ hybrid nanocrystals on an amorphous surface of SiO_2/Si by molecular beam epitaxy. By controlling the quantity of Au atoms deposited onto the SiO_2/Si it is possible to tune the average lateral size of resultant Au–Fe hybrid nanocrystals from 10–20 nm up to 100–150 nm at the same Fe nominal thickness deposited. This process is sensitive to the initial density and size of Au islands. Examination of Au–Fe hybrid nanocrystals obtained was carried out using X-ray diffraction, transmission and scanning electron microscopy, reflection high energy electron diffraction, and Kerr effect methods.

DOI: 10.1134/S1063782618160364

1. INTRODUCTION

Bimetallic magnetic nanomaterials are under extensive investigations now due to their possible application in nanotechnology and nanomedicine. The distinctive characteristic of such materials is their superparamagnetic behaviour, which is important for biomedical, diagnostic and therapeutic applications. At present, the Au–Fe based nanomaterials attract much attention due to higher saturation magnetisation in comparison with the Au–Fe oxide core-shell structures, which synthesis has heavily been investigated over the last decade. Hybrid nanocrystals based on iron, gold or intermetallic $Fe(1-x)Au(x)$ could be promising materials for such applications. Despite the high cost of gold, its insolubility in iron in bulk materials makes it possible to form thin shells on the faces of iron nanocrystals due to phase segregation at high temperatures [1], which allows using the least amount of the expensive metal. Gold provides opportunities for improving the magnetic characteristics of hybrid nanocrystals based on Au–Fe due to its strong spin-orbital coupling and resistance to oxidation. Also, according to [2–6], ordered phases of intermetallics, which have different magnetic characteristics depending on the composition, can exist in nano-sized Au–Fe systems. For instance, Fe_3Au (L12) nanoparticles demonstrate the coercive force of 580 Oe at room temperature, which as well determines possibilities to tune the magnetic properties of hybrid Au–Fe nanocrystals. Another advantage of using iron nanocrystals with a shell of gold or intermetallic compound is the combination of the ferromagnetic and plasmon properties of these two metals [7]. Localised surface plasmon resonance arising in such systems will enhance the magneto-optical effects [8–10]. In the long term, iron silicide nanocrystals, which are similar to the chemical composition of Fe_3Si, can be used instead of pure bcc iron that might increase the magneto-optical response to greater values due to a rise in the spin polarisation [11]. In addition, an increase in the silicon content in ordered nanocrystals of $Fe(3-x)Si(x)$ alloys allows one to increase the coercive force with small losses in the saturation magnetisation [12, 13].

Despite a large number of available works about hybrid nanocrystals based on gold and iron, closer examination hybrid $Fe(1-x)Au(x)/Fe$ systems have not been carried out yet. Usually the study objects in such works are nanocrystals Fe–Au (Fe(core)/Au(shell)) [1, 6, 14] or nanoparticles consisting entirely of $Fe(1-x)Au(x)$ [6, 7, 10], [15–18] intermetallices. Detailed reports in the literature concerning the study of the formation of the hybrid nanocrystal ordered ensembles containing Fe, or iron silicide Fe_3Si, along with the $Fe(1-x)Au(x)$ intermetallic, to the best of our knowledge, are absent. However, combining such materials may lead to the formation of outstanding magnetic

[1] The article is published in the original.

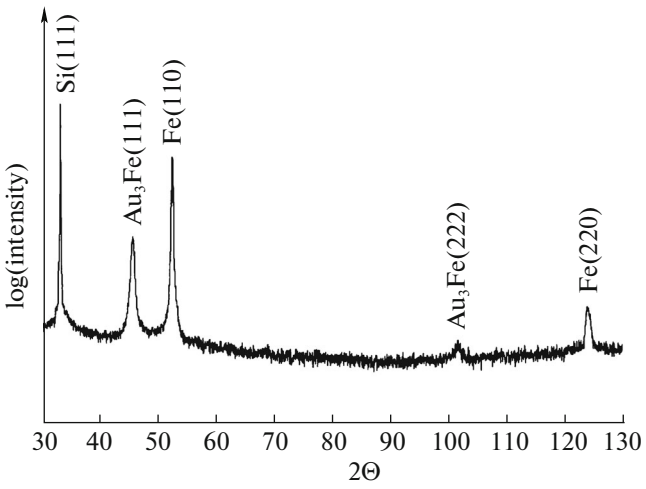

Fig. 1. XRD pattern for $Au_3Fe(111)/Fe(110)$ hybrid nanocrystals obtained with Au layer 11.3 nm thick, the average nanocrystal size of 150–200 nm.

and magneto-optical properties for magnetic recording and magneto-optical applications (recording elements and sensors). Furthermore, the systems, which are the objects of research in this project, may potentially show new effects, which are difficult to foresee at the initial stage.

2. EXPERIMENTAL

Au–Fe/Fe hybrid nanocrystals were prepared on an amorphous surface of SiO_2/Si by molecular beam epitaxy. First Au layer was deposited onto SiO_2/Si at room temperature. The nominal thickness of the Au layer varied in the range from 0 to 11.3 nm. (0, 0.1, 0.5, 0.8, 1, 5.7, 11.3 nm). Further, the nominal thickness value of the Au layer deposited is used for the sample notation. Then, the substrate was heated up to 850°C, and the Fe layer with the nominal thickness of 44 nm was deposited. By controlling the quantity of Au atoms deposited onto the SiO_2/Si we managed to tune the average lateral size of resultant Au–Fe/Fe hybrid nanocrystals from 10–20 nm up to 100–150 nm, and volume fraction of Au–Fe ordered phase at the same Fe nominal thickness deposited.

3. RESULTS AND DISCUSSION

Powder X-ray diffraction (PXRD) investigations were performed on a PANalytical X'Pert Pro MPD diffractometer with a PIXcel detector and a secondary graphite monochromator on CoK_α radiation. The PXRD patterns were collected in the angular range from 30° to 130° 2θ. As it can be noticed in Fig. 1 (XRD pattern for the 11.3 sample) the nanocrystal has a strong texture on Fe(110) and $Au_3Fe(111)$ plane. The lattice parameter of the iron part of nanocrystals corresponds well to the known value of 2.866 Å, whereas Au_3Fe unit cell is slightly bigger than the value available in the literature, 4.02 Å instead of 3.99 Å [1]. This indicates that nonstoichiometric $Au_{3+x}Fe_{1-x}$ intermetallic compound.

RHEED pattern (not shown here) for Au as-grown layer indicates the formation non-textured polycrystalline thin films. RHEED, which is more sensitive technique for small nanoobjects, demonstrates weak reflection of $Au_{3+x}Fe_{1-x}$ phase, such as (112). This reflection can corresponds to the small amount of nanocrystals oriented along one azimuthal direction as it is observed as diffraction spot (Fig. 3 right). Thus, iron deposition step results in texturing of the nanocrystal ensemble. This trend can be noticed on the changes occurred on the RHEED pattern at decrease of the Au layer thickness (not shown). For the 0.5 sample strongest texture can be noticed in several azimuthal directions. Moreover, one can see weak streaks indicating formation of nanocrystals with large flat area. Transformation of dotted spots in the 1 sample to the tick dotted points out that the nanocrystals have highly faceted sides.

Investigation of the sample series obtained with the help of the SEM method reveal the key role of Au layer deposited before Fe evaporation (Fig. 2). Small quantity of Au droplets formed on SiO_2 surface results in

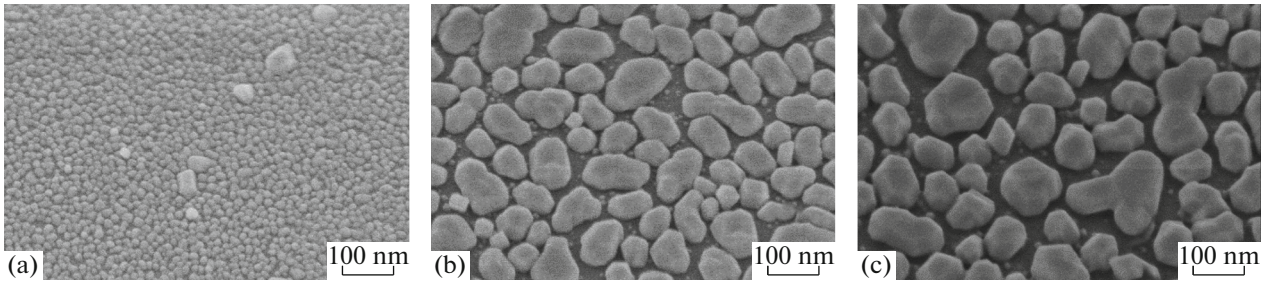

Fig. 2. SEM images $Au_3Fe(111)/Fe(110)$ hybrid nanocrystals grown on $SiO_2/Si(100)$ the nominal Fe layer thickness is 34 nm, Au layer thickness (a) 2 nm, (b) 8 nm, (c) 12 nm (samples tilting is 32°).

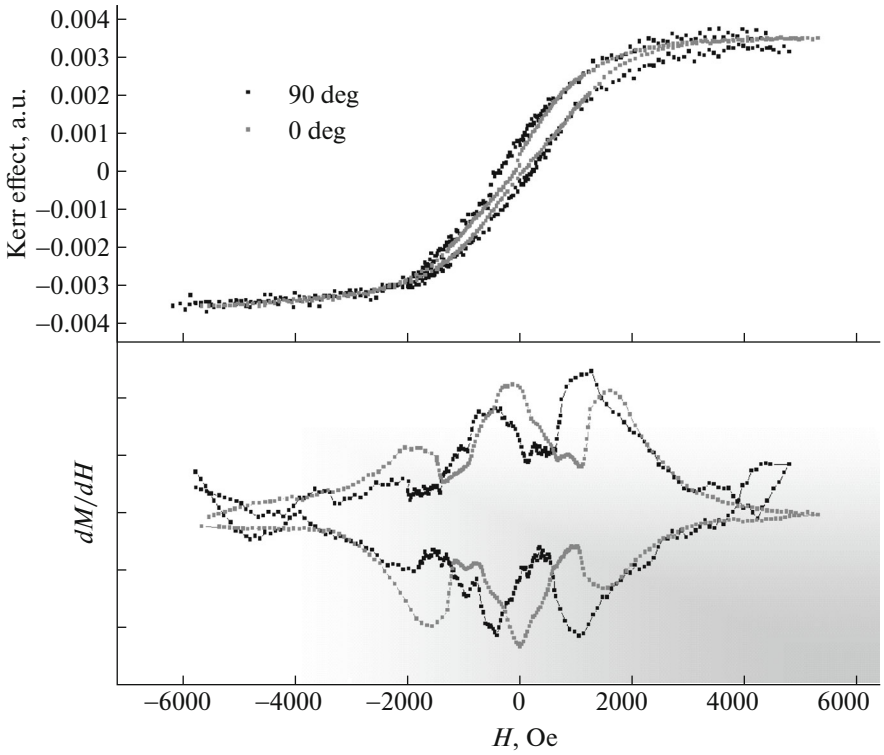

Fig. 3. Hysteresis loops for the 11.3 sample with the magnetic field applied at two perpendicular directions (upper), field derivative of the hysteresis loops (lower).

formation of the nanocrystal ensemble with a lateral size distribution close to the Gauss dependence with the peak center at 30 and 60 nm, for the 0 and 0.1 samples. Further increase in the Au layer thickness (0.5, 0.8, 1 nm), supposedly, results in size inhomogeneous distribution of Au droplets, where one can expect formation of large island due to Oswald ripening while the substrate is heating up to the temperature synthesis. In turn, such inequality causes the formation of two distinguishable fraction of the hybrid nanocrystals due to large gold droplets aggregates more iron atoms incoming. Increase in the Au layer thickness up to 5.7 and 11.3 leads to a strong difference in lateral nanocrystal sizes (Figs. 2b, 2c). Now, small portion volume nanocrystals have sizes in the narrow range from 10 to 20 nm, the rest is spread from 50 to 250 nm. Lateral aspect ratio distribution of the nanocrystals demonstrates their slight elongation. The distribution maximum is at 1.3. The nanocrystal long side direction angle distribution does show strong texture, however, certain increase can be noticed for different angle values over the sample series. Thus, the magnetisation angle dependence at the magnetic field applied parallel to the sample surface should not undergo strong influence of the nanocrystal shape and texture.

Analysis of the TEM images (not shown here) reveals that nanocrystals with small Au fraction have similar size in all three dimensions and approach sphere form whereas the large nanocrystals have large height/width aspect ratio. It can reach values bigger than 3 (not shown here). Estimation of spatial Au and Fe distribution shows that $Au_{3+x}Fe_{1-x}$ compound is mostly situated on sides of the iron nanocrystals forming a nanostructure architecture similar to Janus-like one.

Looking through the magnetic field dependences of the Kerr effect for hybrid Au–Fe nanocrystals we can notice that the form of the hysteresis loop (Fig. 3) is similar for almost all samples (0.5–11.3 nm). They are constricted and have low M_s/M_r ratio. In turn, the 0.1 sample shows the M_s/M_r ratio close to 1; the coercive force is 840 Oe, which is one of the highest value observed for Fe nanoparticle ensembles. Two large magnetization jumps can be observed for the 0.5–11.3 sample. This feature is more noticeable for the sample with high fraction of large flat and textured nanocrystals (0.8 and 0.9 nm). Upon decreasing the applied field from saturation, the first jump takes the magnetization almost from (positive) saturation to a value around zero whereas the second one approaches it to (negative) saturation [19]. A closer look at the 11.3 sample hysteresis loop and it field derivative points out the possible formation of magnetic vortices. The dependence of the vortex annihilation field on an

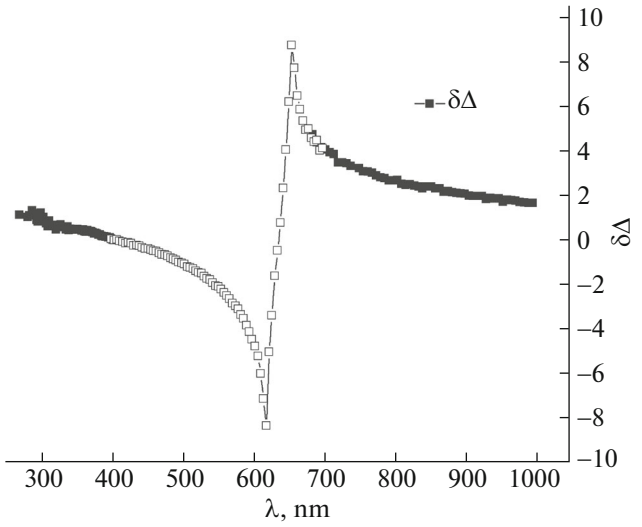

Fig. 4. Wavelength dependence of the magnetoellipsometrical parameter $\delta\Delta = \Delta(+H) - \Delta(-H)$ $Au_3Fe(111)/Fe(110)$ hybrid nanocrystals.

angle can be noticed in Fig. 3. Measurements of magnetoellepsometrical parameters indicating a difference of phase shift of the reflected light at 65 degrees between positive and negative saturation magnetic field show the distinctive resonance feature at 650 nm (Fig. 4). Its location on the wavelength scale can be sensitive to the refractive index of the ambient, which is used for magneto-optic censoring.

4. CONCLUSIONS

Hybrid ferromagnetic Au–Fe nanocrystal ensembles were obtained. When the effective thickness of the Au layer changes from 0 to 11.3 nm, the sizes of Au–Fe nanocrystals obtained vary from 10 to 200 nm with the same thickness of the deposited iron layer at 44 nm. Microscopic data statistical analysis shows that a small number of Au droplets formed on the surface of SiO_2 leads to the formation of an ensemble of nanocrystals with a size distribution close to the Gaussian dependence. The increase in the thickness of the Au layer leads to the formation of larger nanocrystals due to Oswald ripening. Thus, for samples with effective gold thickness of 0.8, 1.0 and 11.3 nm, two groups of Au–Fe nanocrystals with average sizes of 10–20 and 150–200 nm are observed.

At small thicknesses of the pre-deposited Au layer (0.1 nm), as a result of synthesis, one group of nanocrystals with an average size of 30–60 nm is formed at a nominal gold thickness of 0.5 and 5.7 nm.

Nanocrystals corresponding to a gold layer equal to 0.1 nm have the same size in all three dimensions, while large nanocrystals obtained with larger thicknesses of gold layers (1.0–11.3 nm) have aspect ratio (width/height ratio) greater than 3. The aspect ratio of lateral dimensions of the Au–Fe nanocrystals has an average maximum near 1.3 for all samples obtained. On a sample corresponding to the maximum gold thickness, it was shown that the $Au(3-x)Fe(1+x)$ phase is located on the sides of the iron nanocrystals forming a nanoscale Janus-like structure. The average size of the $Au(3-x)Fe(1+x)$ part of the hybrid nanocrystal is 10–20 nm.

An investigation of the field dependences of the magneto-optical Kerr effect showed that a sample with a nominal gold thickness of 0.1 nm demonstrates a M_r/M_s ratio close to 1; the coercive force is 640 Oe. Samples with a high gold content are characterized by the presence of a low value of M_r/M_s close to 0, as well as the asymmetry of the hysteresis loops, which can be caused by the preferred orientation of the nanocrystals in space, and also by the preferred orientation of the $Au(3+x)Fe(1-x)$ with respect to the nanocrystal of pure iron.

The measured spectral dependences of the magnetoellipsometric Kerr effect demonstrate a resonance feature in the photon energy region of the probed emission of 3 eV.

ACKNOWLEDGMENTS

The reported research was funded by Russian Foundation for Basic Research and the government of the region of the Russian Federation, grant no. 18-42-243013, the Program of the President of the Russian Federation for the support of young scientist (СП-2796.2018.1). We also thank L.A. Solovyov for his asistance in XRD analysis.

REFERENCES

1. M. Benoit, N. Tarrat, and J. Morillo, Phys. Chem. Chem. Phys. **18**, 9112 (2016). doi 10.1039/C5CP06258F
2. P. Mukherjee, P. Manchanda, P. Kumar, L. Zhou, M. J. Kramer, A. Kashyap, et al., ACS Nano **8**, 8113 (2014). doi 10.1021/nn5022007
3. J. F. Bondi, R. Misra, X. Ke, I. T. Sines, P. Schiffer, and R. E. Schaak, Chem. Mater. **22**, 3988 (2010). doi 10.1021/cm100705c
4. K. Sato, B. Bian, and Y. Hirotsu, Jpn. J. Appl. Phys., Part 2 Lett. **41**, 1 (2002). doi 10.1143/JJAP.41.L1
5. I. C. Chiang and D. H. Chen, Adv. Funct. Mater. **17**, 1311 (2007). doi 10.1002/adfm.200600525
6. Z. Luo, Y. Vasquez, J. F. Bondi, and R. E. Schaak, Ultramicroscopy **111**, 1295 (2011). doi 10.1016/j.ultramic.2011.04.003
7. K. D. Gilroy, A. Ruditskiy, H. C. Peng, D. Qin, and Y. Xia, Chem. Rev. **116**, 10414 (2016). doi 10.1021/acs.chemrev.6b00211

8. A. F. Kravets, T. I. Borodinova, and V. G. Kravets, J. Opt. Soc. Am. B **33**, 302 (2016). doi 10.1364/JOSAB.33.000302
9. W. Zheng, X. Liu, A. T. Hanbicki, B. T. Jonker, and G. Lüpke, Opt. Mater. Express. **5**, 2597 (2015). doi 10.1364/OME.5.002597
10. V. G. Kravets and A. S. Lapchuk, Appl. Opt. **49**, 5013 (2010). doi 10.1364/AO.49.005013
11. Y. Maeda, T. Ikeda, T. Ichikawa, T. Nakajima, B. Matsukura, T. Sadoh, et al., Phys. Proc. **11**, 200 (2011). doi 10.1016/j.phpro.2011.01.004
12. Y. V. Kudryavtsev, Y. P. Lee, J. Dubowik, and J. Y. Rhee, Phys. Rev. B **68**, 134416 (2003). doi 10.1103/PhysRevB.68.134416
13. J. Karel, J. Juraszek, J. Minar, C. Bordel, K. H. Stone, Y. N. Zhang, et al., Phys. Rev. B **91**, 144402 (2015). doi 10.1103/PhysRevB.91.144402
14. Y. Zhang, Y. H. Wen, Z. Z. Zhu, and S. G. Sun, J. Phys. Chem. C **114**, 18841 (2010). doi 10.1021/jp107709q
15. N. Duxin, N. Brun, C. Colliex, and M. P. Pileni, Langmuir **14**, 1984 (1998). doi 10.1021/la9709094.11
16. J. Padgurskas, I. Prosycevas, R. Rukuiža, R. Kreivaitis, and A. Kupcinskas, Ind. Lubr. Tribol. **64**, 253 (2012). doi 10.1108/00368791211249638
17. Y. I. Petrov, E. A. Shafranovsky, N. S. Perov, A. P. Kuznetsov, and G. V. Karpov, Dokl. Phys. Chem. **449**, 78 (2013). doi 10.1134/S0012501613040076
18. Y. I. Petrov and E. A. Shafranovsky, Int. J. Inorg. Chem. **2012**, 1 (2012). doi 10.1155/2012/610305
19. A. Gomez, F. Cebollada, F. J. Palomares, et al., Appl. Phys. Lett. (2014). doi 10.1063/1.4868401